Available online at www.sciencedirect.com

SciVerse ScienceDirect

Ceramics International 39 (2013) 2309–2315

CERAMICS INTERNATIONAL

www.elsevier.com/locate/ceramint

Impedance spectroscopic studies on $NiFe_2O_4$ with different morphologies: Microstructure vs. dielectric properties

K. Sudalai Muthu[a], N. Lakshminarasimhan[b,*]

[a]Central Instrumentation Facility Division, CSIR-Central Electrochemical Research Institute (CECRI), Karaikudi-630 006, Tamil Nadu, India
[b]Functional Materials Division, CSIR-Central Electrochemical Research Institute (CECRI), Karaikudi-630 006, Tamil Nadu, India

Received 6 August 2012; accepted 27 August 2012
Available online 4 September 2012

Abstract

$NiFe_2O_4$ powders were prepared by combustion synthesis, polyol-mediated and sol–gel methods. Morphological characterization of sintered disks was carried out using scanning electron microscopy (SEM). Dielectric properties of $NiFe_2O_4$ synthesized by different routes were investigated over the frequency range of 100 Hz–5 MHz at room temperature. A difference in dielectric constant (ε_r) and dissipation factor (tan δ) of $NiFe_2O_4$ samples obtained by different synthesis methods has been observed. The observed dissimilarity in the behavior originates from the variation in the microstructure of the samples that is evident in the Cole–Cole plot results.

Keywords: A. Powders: Chemical preparation; B. Electron microscopy; C. Impedance; D. Ferrites

1. Introduction

Materials with high dielectric constant are important components of integrated electronic chips [1,2]. Apart from the dielectric constant, static power and low leakage of current are further necessary [3]. Research focus on the development of such materials is on the rise. Among the various materials, spinel ferrites are fascinating as they comprise of electrically and/or magnetically active transition metal ions [4]. Such significant class of materials are widely used in making of transformers, chokes, microwave absorbers and sensors [5]. Among the ferrites, $NiFe_2O_4$ (NF2O) is an interesting candidate due to its dielectric and magnetoelectric properties and is being used in several applications such as spintronics, satellite communications, memory devices, transformer cores, etc. [6–10]. NF2O having an inverse spinel structure in which Ni^{2+} occupies the octahedral site and half of the Fe^{3+} ions occupy the tetrahedral site formed by the cubic close packing of oxygen atoms and can be represented as $(Fe^{3+})_{Td}[Ni^{2+}Fe^{3+}]_{Oh}O_4$ [11]. However, there is a possibility of reverse cationic distribution in the nanocrystalline spinels in which the random distribution of divalent ion in the T_d and O_h sites has been found [4,12,13].

It is interesting to find the variation in dielectric property of NF2O synthesized by several techniques such as conventional solid state reaction route, sol–gel, microwave synthesis and micro emulsion methods [7,14–16]. Besides, NF2O samples that were synthesized by similar methods exhibit different dielectric constant values [14,17]. Understanding such differences in the property becomes highly important from the technological point of view. The microstructure which is different for samples synthesized by adopting various methods plays a crucial role in controlling the dielectric property of NF2O. Though there are several reports available on the synthesis of NF2O and study of impedance properties, understanding the relation between morphology and dielectric properties of NF2O obtained by different methods is worth investigating. This motivated us to study the role of microstructure on the dielectric property of NF2O by comparing the samples obtained by different routes in a systematic manner. Recently, we have reported the difference in the electrochemical double layer capacitive behavior of NF2O synthesized by adopting different routes such as

*Corresponding author. Tel.: +91 4565 241443; fax: +91 4565 227713.
E-mail addresses: nlnsimha@gmail.com, laksnarasimhan@cecri.res.in (N. Lakshminarasimhan).

0272-8842/$ - see front matter © 2012 Elsevier Ltd and Techna Group S.r.l. All rights reserved.
http://dx.doi.org/10.1016/j.ceramint.2012.08.078

combustion synthesis, polyol-mediated and sol–gel methods and found that the capacitance depends on the morphology [18]. To observe the effect of morphology more directly, in the present study we measured the dielectric property by impedance spectroscopic technique which is a powerful tool in characterizing the electrical properties of grains and grain boundaries.

2. Experimental

2.1. Synthesis

NF2O was synthesized by adopting four different synthesis routes: combustion synthesis using either glycine or alanine as fuel, polyol-mediated and sol–gel methods which are described in detail elsewhere [18]. NF2O samples synthesized by combustion (glycine), combustion (alanine), polyol-mediated and sol–gel methods were named as NF2O-G, NF2O-A, NF2O-P and NF2O-S, respectively. NF2O powder (0.3 g) was pressed into disc shaped samples. The thickness and diameter of each disk are 1.0 mm and 10.0 mm, respectively. All the disks were sintered at 1100 °C in air for 24 h. The surfaces of sintered disks were polished and pasted with the high quality silver on two sides of sample which makes a very good contact with the jaws of impedance analyzer. The silver paste was cured at 400 °C for 10 min.

2.2. Characterization

The phase formation and purity of all the NF2O were examined earlier by powder X-ray diffraction (XRD). The morphologies of sintered NF2O disks were analyzed by scanning electron microscopy (SEM) (S-3000H, Hitachi). Dielectric measurement parameters such as impedance, phase angle, capacitance and dissipation factor were measured at room temperature using a computer controlled impedance analyzer (HIOKI LCR Hi-Tester, Model-3532) in the frequency range of 100 Hz–5 MHz.

From the following empirical equations, the frequency dependent dielectric constant (ε_r), conductivity (σ_{ac}) and resistivity (ρ_{dc}) were calculated at room temperature [19,20]:

$$\varepsilon_r = (Cd/\varepsilon_o A) \quad (1)$$

where ε_r is the dielectric constant, C is the measured capacitance, d is the thickness of the sample and A ($=\pi r^2$) is the area of the sample and ε_o is the permittivity of free space (8.854×10^{-12} Fm^{-1}).

$$\tan\delta = \varepsilon''/\varepsilon' \quad (2)$$

$$\sigma_{ac} = 2\pi f \varepsilon_o \varepsilon'' \quad (3)$$

$$\sigma_{ac} = 2\pi f \varepsilon_o \varepsilon' \tan\delta \quad [\varepsilon'' = \varepsilon' \tan\delta] \quad (4)$$

$$\rho_{dc} = RA/L \quad (5)$$

where ε' is the real part, ε'' is the imaginary part of dielectric constant, δ is the phase angle, f is the frequency, R is the measured resistance of ferrite and L is the thickness of the disk.

3. Results and discussion

3.1. Phase formation and morphological analysis

The single phase formation of NF2O has been confirmed by powder X-ray diffraction technique. The typical XRD pattern of NF2O-S is shown in Fig. 1 along with the standard pattern available in the JCPDS data base and the result confirms the single phase formation. The XRD patterns of all NF2O samples synthesized by different methods were reported elsewhere [18]. The morphologies of sintered NF2O disks obtained by adopting different synthesis routes were analyzed by SEM and the images are shown in Fig. 2. SEM images show that NF2O synthesized by different routes contain different morphologies. NF2O prepared by combustion synthesis exhibits a network with voids and pores. These voids and pores might have formed

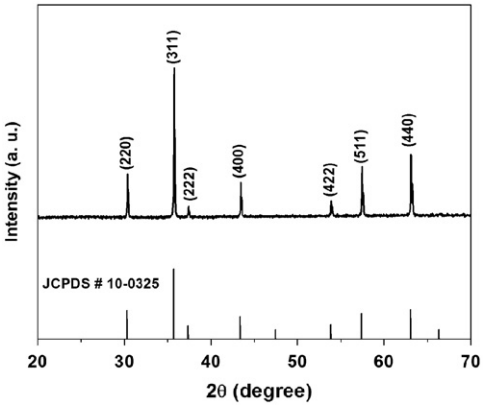

Fig. 1. Powder XRD pattern of NF2O synthesized by sol–gel method is shown along with the standard pattern.

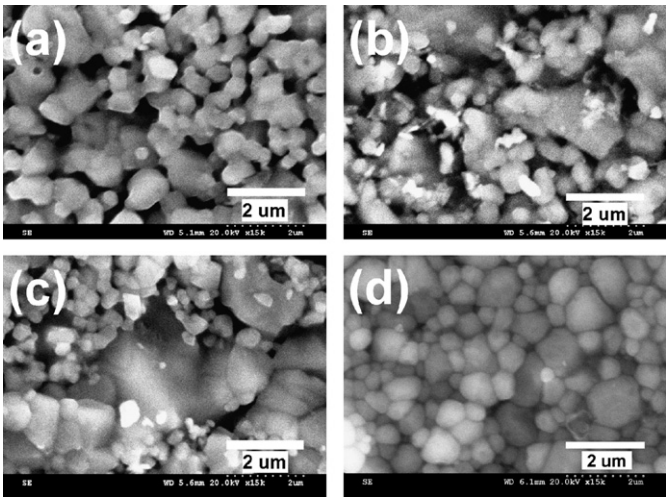

Fig. 2. Scanning electron micrographs (SEM) of sintered disks of (a) NF2O-G, (b) NF2O-A, (c) NF2O-P and (d) NF2O-S.

during the combustion reaction by the escaping gases and present even after sintering. Such a microstructure is known for materials obtained by combustion synthesis [18]. Indivisible grains (i.e. tightly bound and a continuous contact between the grains) without any clear grain boundaries are observed in the SEM image of NF2O-G (Fig. 2a). Micrograph of NF2O-A (Fig. 2b) shows the presence of large and small grains. The microstructure of NF2O-P (Fig. 2c) is related to that of NF2O-A (Fig. 2b). But, the difference between the micro-structure of NF2O-P and NF2O-A is the connectivity among the grains. In the case of NF2O-A, the bulk grains are loosely connected with smaller grains (Fig. 2b). NF2O synthesized by sol–gel method has a negligible inter-grain region as well as low porosity (Fig. 2d). The difference in the morphologies of NF2O synthesized by different methods may influence the dielectric property that originates from grains, grain boundaries and pore structure within the micro structure of a domain system.

3.2. Dielectric properties

The variation in dielectric constant (ε_r) of NF2O synthesized by different routes is shown as a function of frequency in Fig. 3. Frequency dependent dielectric constant (ε_r) of ferrite may reflect the dynamic response behavior of a solid contributed by micro-structural factors [21]. According to Maxwell–Wagner theory and Koop's model, the dielectric material with heterogeneous structure is considered to have well conducting grains separated by highly resistive grain boundaries where the applied voltage drop leads to the building up of space charge polarization [22]. The charge build up at the insulating grain boundary as a consequence of space charge polarization at the electrode–grain interfaces in the lower frequency region is the major contributor to the dielectric behavior of ferrites.

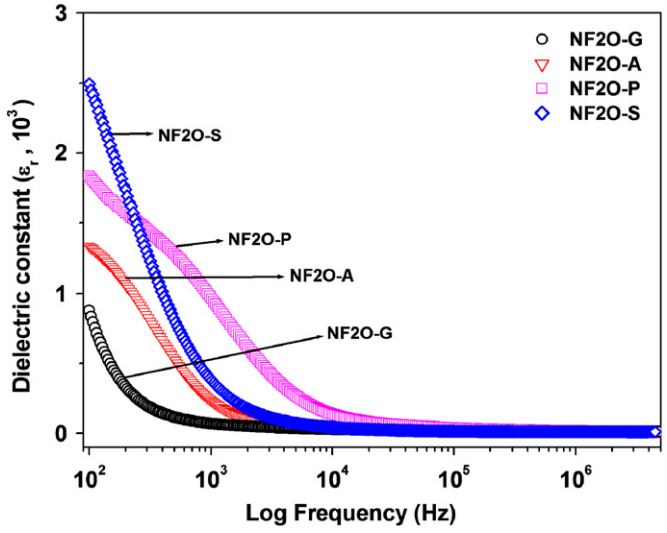

Fig. 3. Frequency variation of dielectric constant of NF2O-G, NF2O-A, NF2O-P and NF2O-S at room temperature.

The dielectric constant, in general, is expected to be high within the sample where the polarization in ferrite is high. From Fig. 3, NF2O-S exhibits the maximum ε_r that may be attributed to the higher polarization or number of space charge carrier (Fe^{2+} ions) than that of in NF2O synthesized by other methods. The low frequency dielectric response in ferrite is strongly affected by the porosity, crystallinity and pore-size distribution within the microstructure [20]. The dielectric constant values at 100 Hz of NF2O synthesized by combustion (Glycine), combustion (Alanine), polyol-mediated and sol–gel methods are 878, 1331, 1833 and 2492, respectively (Table 1). Dielectric constant of NF2O decreases rapidly with increasing frequency and a frequency independent behavior was attained at frequencies above 10^4 Hz. The observed low dielectric constant values of NF2O at higher frequencies are in good agreement with the literature report [23]. This behavior is due to the fact that electron hopping between Fe^{2+} and Fe^{3+} cannot follow the change in external electric field beyond certain frequencies. These results clearly reveal that the observed difference in dielectric constants of NF2O samples at low frequencies is mainly due to grain boundary contributions.

It is observed from Fig. 3 that the variation in ε_r values in NF2O obtained by different methods follows the order: NF2O-G < NF2O-A < NF2O-P < NF2O-S. It is known that ε_r is inversely proportional resistivity [4]. It is interesting to note that NF2O-P despite its low resistivity exhibits a low ε_r (see Table 1). On the other hand, NF2O-S with a negligible inter-grain region as well as low porosity has a higher ε_r. From the morphology and measured dielectric constant, it is understood that a good interconnection between the conducting grains may have the ability to occupy more dipoles/charges than other structures in the low frequency region. It has been recently reported that highly sintered NF2O with less inter-grain region exhibits higher ε_r value than NF2O with other morphological structure [21]. Additionally, NF2O with low porosity, high density and enlarged grains exhibits a high dielectric constant was also reported earlier by Hassan et al. [24].

The dissimilarity in dissipation factor ($\tan\delta$) of NF2O obtained by different methods is shown in Fig. 4. The $\tan\delta$ graph shows peaks with respect to the frequency for all the NF2O samples due to the resonant electron hopping mechanism between two mixed valence cations $Fe(Ni)^{2+}$–$Fe(Ni)^{3+}$ in the octahedral/tetrahedral sites in the spinel crystal structure. The electron/hole hopping between the cations in spinel structure occurs through lattice vibrations due to the localized nature of electrons [4]. It has been found that the hole hopping between Ni^{3+} and Ni^{2+} needs larger activation energies compared to electron hopping between Fe^{2+} and Fe^{3+} ions [4,25]. Hence, the observed dielectric relaxation at room temperature in the present study mainly originates from the electron hopping between Fe^{2+} and Fe^{3+}. NF2O samples synthesized by different routes display peaks at different frequencies indicating the presence of inhomogeneous surface of the electrode. The

Table 1
The calculated ac and dc conductivities of NF2O samples.

Sample	ε_r at 100 Hz	tan δ at 100 Hz	Frequency at 3 kHz			
			$\sigma_{ac}(10^{-5}\ \Omega^{-1}\ cm^{-1})$	ρ_{ac}kΩ cm	$\sigma_{dc}(10^{-7}\ \Omega^{-1}\ cm^{-1})$	ρ_{dc}(MΩ cm)
NF2O-G	878	3.04	1.72	58.1	2.11	4.73
NF2O-A	1331	6.33	6.01	16.6	8.84	1.13
NF2O-P	1833	9.99	11.9	8.40	18.5	0.54
NF2O-S	2492	0.74	3.07	32.5	5.46	1.83

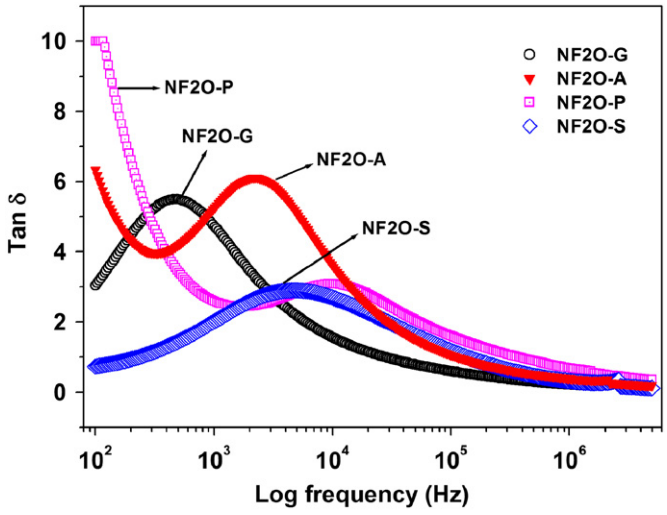

Fig. 4. Variation of dissipation factor (tan δ) of NF2O-G, NF2O-A, NF2O-P and NF2O-S as a function of frequency.

inhomogeneities in NF2O are due to irregularity in grains and grain boundaries, pore structure and inter particle or intra grain connectivity [17,26]. Such inhomogeneties require finite time to line up their axes parallel to an applied electric field and hence the peak will appear at different frequencies. In connection with applied electric field, tan δ is a consequence of lag of polarization. At 10^2 Hz, the tan δ values of NF2O-G, NF2O-A, NF2O-P and NF2O-S are 3.04, 6.33, 9.99 and 0.74, respectively. The value of tan δ for NF2O-P exhibits a systematic decrease with increasing frequency (9.99 at 10^2 Hz, 2.63 at 10^3 Hz and 0.763 at 10^6 Hz). The high loss in NF2O-P may originate from the higher conductivity causing the higher leakage current (see Table 1).

Fig. 5 shows the Cole–Cole plots of NF2O-G, NF2O-A, NF2O-P and NF2O-S. Two distinct parameters are observed from the Cole–Cole plot. The primary one is ohmic (R_Ω) and polarization resistance (R_p) and the second one is how the grains and grain boundaries interact with frequency within the microstructure. The high and low frequency intercepts on the real axis points to the R_Ω and total resistance (R_t), respectively. The polarization resistance (R_p), is the electrode reaction kinetics accommodated with grain boundaries, calculated from the following relation [27]:

$$R_p = (R_t - R_\Omega) \tag{6}$$

Dielectric material's microstructure can be assumed to consist of parallel conducting plates (grains) separated by resistive plates (grain boundaries). In the Cole–Cole plot of NF2O, a semi-circular arc in the low frequency region represents grain boundary contributions and the arc in the high frequency side corresponds to the bulk (or grain) contribution. Two characteristic features can be clearly observed from the Cole–Cole plots of NF2O samples. Primarily two depressed semi-circular arcs are observed with NF2O-A and NF2O-P both of which have smaller and larger grains, clear grain boundaries along with micropores and well resolved inter-grain regions. Secondly, NF2O-G and NF2O-S having negligible inter-grain region or indivisible conducting grains and good connectivity between inter grains exhibit a single depressed semi-circular arc. The observed non-ideal behavior in the Cole–Cole plot can be due to the inhomogeneties in the microstructure of the NF2O and this gives rise to constant phase element (CPE) instead of capacitance for all the cases. The CPE represents the occurrence of several relaxation processes with similar relaxation time [28,29]. The CPE with impedance is expressed as:

$$Z(w) = 1/Q(iw)^n \tag{7}$$

where $i = \sqrt{-1}$, $0 < n < 1$, and Q is a constant with dimension Fs^{n-1}. More complicated frequency response than a simple undistributed RC time constant process exhibited by the CPE which is used to accommodate the non-ideal behavior of the capacitance that may have a pure resistive or capacitive behavior if the value is either zero or unity, respectively.

A careful attention is indispensable to explore the physical parameters of prepared NF2O disks. The parameters such as grain resistance (R_g), grain boundary resistance (R_{gb}), and the CPE contribution from grain (Q_g) and grain boundaries (Q_{gb}) were obtained at room temperature by fitting the Cole–Cole plots using PAS-IM6 Electrochemical Impedance Analyzer-Thales 4.18 USP software (within 1% fitting error) and the measured values are listed in Table 2. The ohmic or contact resistance (R_Ω) contributions were omitted for all the cases.

The Cole–Cole plot of NF2O-G as a function of frequency is shown in Fig. 5a. Here, the spectrum shows a single depressed semi-circular arc implying the contributions from conducting grains. The grain boundaries' contribution cannot be resolved but an additional impedance response (like a tail) is appeared in the low frequency region and this behavior is similar to the result reported in the literature [7].

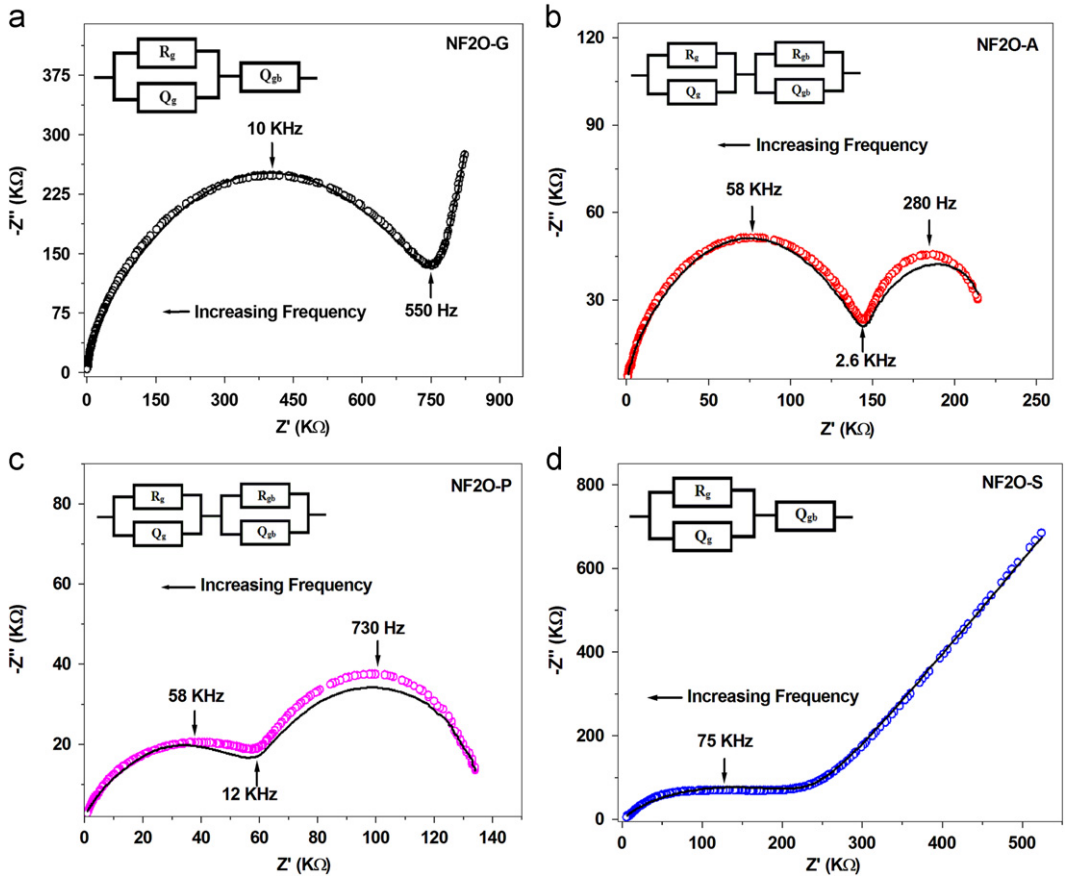

Fig. 5. Cole–Cole plot of (a) NF2O-G, (b) NF2O-A, (c) NF2O-P and (d) NF2O-S in the frequency range of 100 Hz–5 MHz at room temperature and the corresponding equivalent circuit models are shown in the inset.

Table 2
The calculated resistance and CPE values from the Cole–Cole plots of NF2O samples.

Sample	Bulk region			Grain boundary		
	R_g(kΩ)	CPE1		R_{gb}(kΩ)	CPE2	
		Q_g(nF)	n_g		Q_{gb}(nF)	n_{gb}
NF2O-G	778.8	0.43	0.81	–	15.13	0.88
NF2O-A	146.2	0.32	0.83	93.8	13.65	0.72
NF2O-P	60.9	1.50	0.74	81.7	9.005	0.75
NF2O-S	233.2	0.97	0.86	–	11.72	0.64

The microstructure of NF2O-G (see Fig. 2a) consists of indivisible grains and indistinct grain boundaries that may influence the property as clearly observed by the disappearance of second semi-circular arc in the Cole–Cole plot. Such indivisible grains along with pores in NF2O-G result in the observed very large total resistance. In order to correlate the electrical properties of NF2O-G, the data has been fitted with an equivalent circuit model of $(R_gQ_g)(Q_{gb})$ which is shown in inset Fig. 5a.

NF2O-A exhibits two semi-circular arcs in the Cole–Cole plot. The corresponding electrical circuit of NF2O-A was fitted based on the equivalent circuit model of $(R_gQ_g)(R_{gb}Q_{gb})$ which is shown in the inset in Fig. 5b. The measured R_{gb} and R_g are 93.8 and 146.2 kΩ, respectively, from which we could confirm that the contribution from the thin grain boundary is low when compared to grain contribution. The microstructure of NF2O-A (Fig. 2b) indicates that the conducting grains are larger than the insulating grain boundary region and hence the contribution from the grain boundaries to the resistance and CPE is small.

The Cole–Cole plot of NF2O-P shows two depressed semi-circular arcs and the result is fitted with an equivalent circuit as shown in Fig. 5c. The observed result with NF2O-P is quite opposite to that of NF2O-A. The grain boundary contribution in NF2O-P is predominant whereas the resistance of grain is a major contributor in the case of NF2O-A as shown in the difference in the radius of semi-circular arcs in these two cases. The obtained results are in good correlation with the morphology of NF2O-P that shows the presence of both larger and smaller sized grains with difference in the nature of grain boundaries. The radius of the second semi circular arc (at lower frequencies) is larger than the first one revealing that the contribution from grain boundary (R_{gb}) is more as it contains a large number of smaller grains. Such smaller grains are well connected with the larger ones which provide a continuous pathway for transport of charge carriers through the electrodes and thereby lead to an increase in conductivity. This kind of micro-structure is desirable for providing

maximum conductivity ($\sigma_{dc}=18.5\times10^{-7}\,\Omega^{-1}\,cm^{-1}$) than other NF2O microstructure.

NF2O-S shows (Fig. 5d) an apparently depressed semi-circular arc in the high frequency region. Low frequency tail is due to the diffusive response by blocking the charge carries by the well connected inter-grain region and the results are fitted with an equivalent circuit model consisting of a parallel combination of R_g and Q_g elements corresponds to high frequency region, connected in series with Q_{gb}. The surface roughness like the close connection between the grains is an important contributor to the observed depressed semi-circle. The individual contribution effect of grain boundary disappeared by grain growth which decreases the porosity and grain boundaries. The present study reveals the difference in the dielectric properties of NF2O with different morphological structures and a clear understanding of conduction mechanism in all the cases needs further exploration.

4. Conclusions

In the present study, the dielectric behavior of $NiFe_2O_4$ samples synthesized by different methods has been compared. Among the samples studied, $NiFe_2O_4$ synthesized by sol–gel method exhibited a high dielectric constant of 2492 and low dielectric loss of 0.74 suggesting its potential application for integrated electronic chips. The results reveal a difference in the dielectric constant of $NiFe_2O_4$ which is morphology dependent. The dissimilarity in the grain and grain boundary structure is responsible for the observed difference in dielectric constant and relaxation process. This work with systematic evaluation of dielectric properties of $NiFe_2O_4$ by control of microstructure reveals the importance of morphology in fine tuning the property.

Acknowledgments

The author KSM acknowledges the Council of Scientific and Industrial Research (CSIR), New Delhi for research assistantship through CSIR-Diamond Jubilee Research Intern program. Central Instrumentation Facility (CIF) of CSIR-CECRI and Dr. Shahid Anwar are acknowledged for characterization facilities.

References

[1] A.P. Ramirez, M.A. Subramanian, M. Gardel, G. Blumberg, D. Li, T. Vogt, S.M. Shapiro, Giant dielectric constant response in a copper-titanate, Solid State Communications 115 (2000) 217–220.

[2] T. Zhou, J.W. Zha, R.Y. Cui, B.H. Fan, J.K. Yuan, Z.M. Dang, Improving dielectric properties of $BaTiO_3$/ferroelectric polymer composites by employing surface hydroxylated $BaTiO_3$ nanoparticles, ACS Applied Materials & Interfaces 3 (2011) 2184–2188.

[3] K. Maex, M.R. Baklanov, D. Shamiryan, F. Iacopi, S.H. Brongersma, Z.S. Yanovitskaya, Low dielectric constant materials for microelectronics, Journal of Applied Physics 93 (2003) 8793–8841.

[4] J.S. Kim, K.H. Lee, C.I. Cheon, Crystal structure and the effect of annealing atmosphere on the dielectric properties of the spinels $MgAl_2O_4$, $NiFe_2O_4$, and $NiAlFeO_4$, Journal of Electroceramics 22 (2009) 233–237.

[5] J. Jacob, M. Abdul Khadar, A. Lonappan, K.T. Mathew, Microwave dielectric properties of nanostructured nickel ferrite, Bulletin of Materials Science 31 (2008) 847–851.

[6] U. Lüders, A. Barthélémy, M. Bibes, K. Bouzehouane, S. Fusil, E. Jacquet, J.-P. Contour, J.-F. Bobo, J. Fontcuberta, A. Fert, $NiFe_2O_4$: a versatile spinel material brings new opportunities for spintronics, Advanced Materials 18 (2006) 1733–1736.

[7] K. Kamala Bharathi, G. Markandeyulu, C.V. Ramana, Impedance spectroscopic characterization of Sm and Ho doped Ni ferrites, Journal of the Electrochemical Society 158 (2011) G71–G78.

[8] K. Kamala Bharathi, G. Markandeyulu, C.V. Ramana, Structural, magnetic, electrical, and magnetoelectric properties of Sm- and Ho-substituted nickel ferrites, Journal of Physical Chemistry C 115 (2011) 554–560.

[9] K. Kamala Bharathi, M. Noor-A-Alam, R.S. Vemuri, C.V. Ramana, Correlation between microstructure, electrical and optical properties of nanocrystalline $NiFe_{1.925}Dy_{0.075}O_4$ thin films, RSC Advances 2 (2012) 941–948.

[10] M.A.F. Ramalho, L. Gama, S.G. Antonio, C.O. Paiva-Santos, E.J. Miola, R.H.G.A. Kiminami, A.C.F.M. Cost, X-ray diffraction and Mössbauer spectra of nickel ferrite prepared by combustion reaction, Journal of Materials Science 42 (2007) 3603–3606.

[11] A.F. Wells, Structural Inorganic Chemistry, third ed., Oxford University, London, 1962.

[12] R.S. Turtelli, M. Atif, N. Mehmood, F. Kubel, K. Biernacka, W. Linert, R. Grössinger, Cz. Kapusta, M. Sikora, Interplay between the cation distribution and production methods in cobalt ferrite, Materials Chemistry and Physics 132 (2012) 832–838.

[13] J. Jacob, M.A. Khader, Investigation of mixed spinel structure of nanostructured nickel ferrite, Journal of Applied Physics 107 (2010) 114310.

[14] M. Younas, M. Nadeem, M. Atif, R. Grossinger, Metal–semiconductor transition in $NiFe_2O_4$ nanoparticles due to reverse cationic distribution by impedance spectroscopy, Journal of Applied Physics 109 (2011) 093704.

[15] D. Zhang, Z. Tong, G. Xu, S. Li, J. Ma, Templated fabrication of $NiFe_2O_4$ nanorods: characterization, magnetic and electrochemical properties, Solid State Sciences 11 (2009) 113–117.

[16] D.-H. Chen, X.-R. He, Synthesis of nickel ferrite nanoparticles by sol-gel method, Materials Research Bulletin 36 (2001) 1369–1377.

[17] S. Narendra Babu, J.-H. Hsu, Y.S. Chen, J.G. Lin, Dielectric, magnetic and magnetoelectric properties of multiferroic $BiFe_{0.5}Cr_{0.5}O_3$–$NiFe_2O_4$ composites, Journal of Applied Physics 107 (2010) 09D919.

[18] Shahid Anwar, K. Sudalai Muthu, V. Ganesh, N. Lakshminarasimhan, A comparative study of electrochemical capacitive behavior of $NiFe_2O_4$ Synthesized by different routes, Journal of the Electrochemical Society 158 (2011) A976–A981.

[19] E.V. Gopalan, K.A. Malini, S. Saravanan, D.S. Kumar, Y. Yoshida, M.R. Anantharaman, Evidence for polaron conduction in nanostructured manganese ferrite, Journal of Physics D: Applied Physics 41 (2008) 185005.

[20] S. Nasir, G. Asghar, M.A. Malik, M. Anis-ur-Rehman, Structural, dielectric and electrical properties of zinc doped nickel nanoferrites prepared by simplified sol–gel method, Journal of Sol–Gel Science and Technology 59 (2011) 111–116.

[21] S. Choudhury, M.A. Bhuiyan, S.M. Hoque, Effect of sintering temperature on apparent density and transport properties of $NiFe_2O_4$: synthesized from nano size powder of NiO and Fe_2O_3, International Nano Letters 1 (2011) 111–116.

[22] A.D. Sheikh, V.D. Mathe, Anomalous electrical properties of nanocrystalline Ni–Zn ferrite, Journal of Materials Science 43 (2008) 2018–2025.

[23] G.R. Mohan, D. Ravinder, A.V. Ramana Reddy, B.S. Boyanov, Dielectric properties of polycrystalline mixed nickel–zinc ferrites, Materials Letters 40 (1999) 39–45.

[24] J. Hassan, F.M. Yen, M. Hashim, Z. Abbas, Z. Abdul Wahab, W.M.D.W. Yusoff, A. Zakaria, Dielectric permittivity of nickel ferrites at microwave frequencies 1 MHz to 1.8 GHz, Ionics 13 (2007) 219–222.

[25] N. Sivakumar, A. Narayanasamy, N. Ponpandian, J.-M. Greneche, K. Shinoda, B. Jeyadevan, K. Tohji, Effect of mechanical milling on the electrical and magnetic properties of nanostructured $Ni_{0.5}Zn_{0.5}$-Fe_2O_4, Journal of Physics D: Applied Physics 39 (2006) 4688–4694.

[26] D.R. Patil, S.A. Lokare, R.S. Devan, S.S. Chougule, Y.D. Kolekar, B.K. Chougule, Dielectric properties and magnetoelectric effect of $(x)NiFe_2O_4+(1-x)Ba_{0.8}Sr_{0.2}TiO_3$ composites, Journal of Physics and Chemistry of Solids 68 (2007) 1522–1526.

[27] Qing Xu, Kai Zhao, Duan-Ping Huang, Bok-Hee Kim, Min Chen, Hong Wang, Electrode properties of porous $La_2NiO_{4+\delta}$ layers screen-printed on a $Ce_{0.9}Sm_{0.2}O_{2-\delta}$ electrolyte, Journal of Ceramic Processing Research 10 (2009) 202–207.

[28] E. Barsoukov, J. Ross Macdonald, Impedance Spectroscopy-Theory, Experiment and Applications, John Wiley & Sons, New Jersey, 2005.

[29] J. Bisquert, G. Garcia-Belmonte, P. Bueno, E. Longo, L.O.S. Bulhoes, Impedance of constant phase element (CPE)-blocked diffusion in film electrodes, Journal of Electroanalytical Chemistry 452 (1998) 229–234.